Journal of Orthopaedic Surgery and Research

RESEARCH

Open Access

Sodium alginate microspheres loaded with Quercetin/Mg nanoparticles as novel drug delivery systems for osteoarthritis therapy

Jun Chen[1†], Guoya Wu[1†], Jian Wu[1] and Zhijian Jiao[1*]

Abstract

Background Osteoarthritis (OA) is the most prevalent arthritic disease characterized by cartilage degradation and low-grade inflammation, for which there remains a lack of efficacious therapeutic interventions. Notably, mitigating the impact of oxidative stress (OS) and inflammatory factors could help alleviate or hinder the advancement of OA. Given the benefits of both quercetin (Que) and Magnesium ion (Mg^{2+}) in OA treatment, coupled with the structural properties of Que, we have innovatively developed the Que-Mg^{2+} nanoparticles (NPs), aiming to deliver both Que and Mg^{2+} simultaneously and achieve enhanced therapeutic outcomes for OA. Moreover, to avoid the adverse reactions linked to frequent injections, sodium alginate (SA) microspheres encapsulating Que-Mg^{2+} NPs (Que-Mg@SA) were designed to treat the H_2O_2-induced OA cell model.

Methods Que-Mg@SA microspheres were synthesized using the ionotropic gelation technique, with calcium chloride acting as the cross-linking agent. Comprehensive characterization of the Que-Mg@SA was conducted through transmission electron microscope (TEM), dynamic light scattering (DLS), optical microscope, and scanning electron microscope (SEM), which provided detailed insights into their size, zeta potential, morphology, and micromorphology. Additionally, the microsphere swelling rate and Que release were evaluated. The biocompatibility of Que-Mg@SA microspheres, along with their impact on chondrocyte viability, were detected through CCK-8 assay and live/dead cell staining. Furthermore, the antioxidant and anti-inflammatory properties of Que-Mg@SA were evaluated by examining the ROS scavenging ability and pro-inflammatory factors levels, respectively. Finally, the regulatory influence of Que-Mg@SA microspheres on extracellular matrix (ECM) metabolism in OA was assessed by immunofluorescence staining and Western blot.

Results Characterization results revealed that Que-Mg NPs exhibit nanoscale diameter, exceptional stability, and good dispersibility, while Que-Mg@SA possesses high entrapment efficiency (EE%) and loading efficiency (LE%), pronounced hygroscopic properties, and sustained drug-release capabilities. Additionally, in vitro cellular assays

[†]Jun Chen and Guoya Wu contributed equally to this work and should be considered co-first authors.

*Correspondence:
Zhijian Jiao
chenj0129@163.com

Full list of author information is available at the end of the article

revealed that the biocompatible Que-Mg@SA microspheres significantly restored chondrocyte viability, scavenged H_2O_2-induced excessive ROS, reduced the levels of inflammatory cytokines, upregulated cartilage anabolic gene expression, downregulated cartilage catabolic protease gene expression, and maintained the metabolic balance of cartilage tissue.

Conclusion The functionalized Que-Mg@SA microspheres developed in our study hold great promise as a drug delivery system for OA and potentially other biomedical applications.

Clinical trial number Not applicable.

Graphical abstract

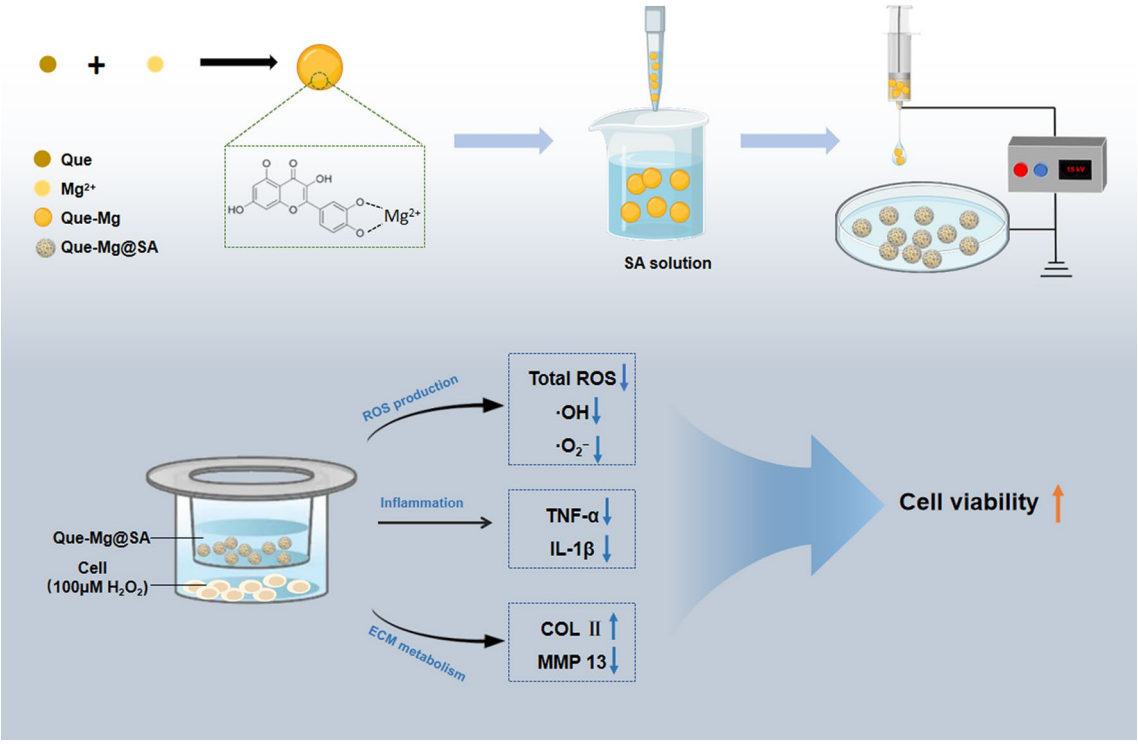

Keywords Osteoarthritis, Sodium alginate microspheres, Quercetin, antioxidant, Anti-inflammatory, Extracellular matrix

Introduction

Osteoarthritis (OA), the most prevalent degenerative joint disorder, is marked by cartilage degradation and low-grade inflammation and is projected to impact approximately 78 million individuals globally by 2040 [1, 2]. Currently, pharmacological and surgical interventions represent the conventional approaches for OA [3, 4]. However, pharmacological treatments primarily aim at pain relief and anti-inflammation, with clinical outcomes often hindered by notable adverse reactions [5] and limited cartilage-targeted absorption or accumulation at the OA cartilage site. Surgical treatments are constrained by the challenges of fibrocartilage regeneration, the scarcity of donor tissues or chondrocytes, complications arising from extensive cartilage damage or advanced OA, and the risk of second surgery [6]. Present treatment options remain far from curative, largely offering palliative relief. Consequently, there is a critical need for therapeutic strategies capable of slowing disease progression and improving both bone and joint function.

Chondrocytes, the only cell type in cartilage tissue, play a vital role in maintaining the structural integrity of cartilage [7, 8]. In addition, excessive production of reactive oxygen species (ROS) by chondrocytes is a key contributor to the progression of OA. ROS-regulated pro-inflammatory factors promote cartilage degradation by triggering the secretion of substantial quantities of matrix metalloproteinases (MMPs) while simultaneously

suppressing the synthesis of extracellular matrix (ECM) [9, 10]. Given this, mitigating the impact of oxidative stress (OS) and inflammatory factors could help alleviate or hinder the advancement of OA.

Flavonoids, widely found in fruits and vegetables, are natural compounds with various pharmacological properties, including antioxidative, anti-inflammatory, and anticancer properties [11, 12]. Among these, quercetin (Que) as one of the most abundant flavonoids, has shown remarkable therapeutic potential for joint-related disorders, particularly OA [13]. Preclinical studies have highlighted Que's anti-arthritic properties and protective effects on joints [14]. Moreover, it has been reported that Que prevents and treats OA by modulating the expression of inflammatory factors, while also alleviating articular cartilage degeneration by reducing OS and inhibiting ECM degradation in cartilage [15]. Overall, Que appears to be a promising candidate for OA due to its multifaceted mechanisms of action. However, the clinical application of Que is hindered by several limitations, including a pronounced first-pass elimination, low bioavailability, and poor water solubility. Moreover, the short retention time and rapid clearance of drugs from the joint further restrict the efficacy of Que [16]. To overcome these challenges, synergistic interactions involving active groups, such as metal ions, show potential for enhancing the solubility and bioavailability of Que, thereby enhancing its therapeutic efficacy.

Magnesium (Mg) is primarily stored in the skeletal system and is essential for maintaining the health of bone and cartilage [17]. Studies have shown the connection between the Mg ion (Mg^{2+}) deficiency and OA progression [18]. For the past few years, Mg-based biomaterials have demonstrated significant translational potential in OA due to their excellent tissue compatibility and pro-osteogenic properties following implantation [19, 20]. Yao et al. have reported that Mg^{2+} mitigates cartilage degeneration in OA by modulating cartilage matrix synthesis [21]. Considering its cost-benefit and safety profile, Mg^{2+} holds tremendous clinical application value. Given the benefits of both Que and Mg^{2+}, along with the structural properties of Que, we have innovatively developed the Que-Mg^{2+} nanoparticles (NPs), aiming to deliver both Que and Mg^{2+} simultaneously and achieve enhanced therapeutic outcomes for OA.

In contrast to systemic delivery, intra-articular administration of nanomaterials is a more prevalent approach for the management of OA [22], primarily because direct injection into the joint markedly reduces the required drug dosage and results in more effective therapeutic outcomes. To avoid the adverse reactions linked to frequent injections, an appropriate drug delivery system is essential. Alginates is an injectable biopolymer that has been applied to targeted drug delivery systems and tissue engineering, with broad application prospects [23]. Among them, sodium alginate (SA) stands out as one of the most extensively studied types, particularly in the pharmaceutical and biomedical fields. Its great biodegradability, biocompatibility, non-immunogenicity, non-toxicity, affordability, and ease of production [24] have established it as a key polymer material for preparing microspheres [23].

Building on the aforementioned considerations, SA microspheres encapsulating Que-Mg^{2+} NPs (Que-Mg@SA) were designed and synthesized for the treatment of the OA cell model. The synthesized microspheres were characterized in terms of size, morphology, zeta potential, microsphere swelling rate, and Que release profile. Additionally, the therapeutic potential of Que-Mg@SA microspheres was evaluated by assessing chondrocyte viability, as well as their antioxidant and anti-inflammatory impacts on OA. It is hypothesized that the Que-Mg@SA developed in this study may offer a straightforward and promising strategy for inhibiting the progression of OA by scavenging ROS, combating inflammation, and regulating ECM metabolism.

Materials and methods

Materials

Que, NaOH, $MgCl_2{\cdot}6H_2O$, SA, $CaCl_2$, Tween 80, PBS, and H_2O_2 were obtained from Aladdin (Shanghai, China). Calcein-AM/propidium iodide (PI) assay kit was obtained from Sigma (USA), CCK-8 assay kit, 2′, 7′-dichlorofluorescein diacetates (DCFH-DA), dihydroethidium (DHE), paraformaldehyde (4%), and Triton X-100 (0.1%) were obtained from Beyotime (Shanghai, China). Alexa 488 secondary antibody, and hydroxyphenyl fluorescein (HPF) were obtained from Thermo Fisher (USA). 4′,6-diamidino-2-phenylindole (DAPI), bovine serum albumin (5%, BSA), TNF-α ELISA kit, IL-1β ELISA kit, were obtained from Solarbio (Beijing, China). Primary antibodies for matrix metalloprotease 13 (MMP13), Collagen type II (COL II), TNF-α, IL-1β, and GADPH were obtained from Affinity (Jiangsu, China). Sodium dodecyl sulfate (SDS), polyvinylidene fluoride (PVDF) membrane, tris-buffered saline (TBS), and skimmed milk were obtained from Servicebio (Wuhan, China).

Preparation of Que-Mg NPs

A total of 120 mg of Que was dissolved in 30 mL of NaOH solution, followed by the addition of 5 mL $MgCl_2{\cdot}6H_2O$ solution (10 mg/mL). The resulting mixture was sonicated (500 W) via JIUGONG sonicator (JG28K15, China) for 15 min, then centrifuged by Lu Xiangyi Centrifuge (TGL-16 M, China) at 12,000 r/min for 15 min, and washed twice with deionized water. The NPs obtained were then subjected to dialysis in deionized water for 48 h using dialysis tubing (FDM303, Beyotime, China)

with a molecular weight cut-off of 3500 Da to eliminate excess metal ions and NaOH. Finally, the Qu-Mg NPs solution was stored at 4 °C.

Preparation of SA microspheres and Que-Mg@SA microspheres

Que-Mg@SA microspheres were synthesized using the ionotropic gelation technique, with calcium chloride acting as the cross-linking agent as described previously [25]. The overnight-stirred 20 mL SA solution (1.5%) was filtered through a 0.22 μm membrane and transferred into a clean centrifuge tube. It was then loaded into a sterile threaded syringe, connected to the needle and hose. With the electrostatic spinning apparatus (Dongwen High Voltage, China) fully assembled, microspheres were collected in a receiving dish containing 2% $CaCl_2$ solution. The apparatus was set to a flow rate of 0.8 mL/h and a voltage range of 13–15 kV, allowing stable microsphere spraying without spattering through fine voltage adjustments. The collected microspheres were washed three times with pure water to yield the SA microspheres. Separately, the previously prepared Que-Mg NPs were dispersed into a 1.5% SA solution (2 mg/mL Que content), and the Que-Mg@SA microspheres were produced following the same procedure.

Characterization of Que-Mg NPs and Que-Mg@SA microspheres

The samples were prepared by depositing Que-Mg NPs onto a copper grid, followed by drying at room temperature. The morphological characteristics of the Que-Mg NPs were then observed using a transmission electron microscope (TEM; FEI Talos F200S, FEI) operated at 100 kV. The size and zeta potential of Que-Mg NPs were measured via dynamic light scattering (DLS). Moreover, the morphology and particle size of SA microspheres and Que-Mg@SA microspheres were compared through an optical microscope. In addition, the micromorphology of Que-Mg@SA microspheres was further observed with a scanning electron microscope (SEM, Hitachi SU8010).

Entrapment efficiency% (EE%) and loading efficiency% (LE%) of Que in microspheres

Precisely 10 mg of Que-Mg@SA microspheres were weighed into a centrifuge tube, to which a mixture of acetonitrile and 1% formic acid in water (35:65, v/v, 5 mL) was added. The amount of Que in the solution was quantified by a high performance liquid chromatography (HPLC; Agilent 1260, Agilent Technologies, USA). The EE% and LE% were then calculated using the following equations:

$$EE\,(\%) = \frac{\text{mass of drug entrapped in microspheres}}{\text{mass of drug fed}} \times 100\%$$

$$LE\,(\%) = \frac{\text{mass of drug entrapped in microspheres}}{\text{mass of microspheres with drug entrapped}} \times 100\%$$

Swelling ratio study

A specified number of Que-Mg@SA microspheres was weighed and dispersed into a centrifuge tube containing 10 mL of PBS. The tube was then placed in a constant temperature shaker at 37 °C, set to 100 rpm, allowing the Que-Mg@SA microspheres to swell in PBS fully. At various time intervals, the swollen Que-Mg@SA microspheres were removed, and their mass was measured through an electronic balance. The swelling rate (Q) of the Que-Mg@SA microspheres was calculated using the following formula.

$$Q\,(\%) = \frac{M2 - M1}{M1} \times 100\%$$

Where M2 referred to the mass of the swollen Que-Mg@SA, and M1 referred to the initial mass of Que-Mg@SA.

Drug release studies

The in vitro drug release rates of free Que and Que-Mg@SA microspheres were evaluated. Both Que solution and Que-Mg@SA microspheres were encapsulated in dialysis bags (3500 Da) and immersed in 20 mL of PBS containing 0.2% Tween 80. Considering the acidic microenvironment of OA (pH = 6.6–7.2) [26], a pH of 6.8 was selected for the in vitro release experiments here. The setup was placed in a shaker at 37 °C and 100 rpm for the drug release study. At predetermined time points (1, 2, 4, 8, 12, 18, 24, 30, and 36 h), 1 mL sample was withdrawn, with the same volume of fresh PBS solution replenished at the same temperature. The released Que was quantified by HPLC with an Agilent C18 column (200 × 4.6 mm; 5 mm particle size) operated at 25 °C. Absorbance was measured using ultraviolet-visible (UV-Vis) spectroscopy (CARY 5000, Agilent Technologies, USA) at 370 nm, and the concentration of Que was determined based on a standard calibration curve ($Y = 65.121 + 114.42$, $R^2 = 0.9988$; Fig. S1). The drug release percentage (%) was calculated using the following equation.

$$S\,(\%) = \frac{\sum^{\text{n-1}}_{i=1} V_a C_i + V_0 C_n}{M} \times 100\%$$

Where V_0 referred to the total volume of release medium ($V_0 = 20$ mL), V_a referred to the sampling volume ($V_a = 1$ mL), C_n referred to the concentration of Que at the n^{th} sampling, and M referred to the total amount of Que.

OA cell model

The rat chondrocytes were purchased from Wuhan Sunncell Biotechnology Co., Ltd (Wuhan, China). To

simulate the environment of excess ROS present in OA, chondrocytes were seeded in the lower chambers of Transwell plates and exposed to 100 μM H_2O_2. The subsequent experiments were categorized into six groups: the Control group (PBS), the model group (H_2O_2), and four administration groups, including H_2O_2 + Que, H_2O_2 + Que-Mg, H_2O_2 + SA, and H_2O_2 + Que-Mg@SA. Based on the concentration screening results from the preliminary experiment shown in Fig. S2, the administered dose of Que was determined to be 30 μM.

Live/dead cell staining

To evaluate the biosafety of different materials and their effects on chondrocyte survival, live/dead cell staining was performed via a Calcein-AM/propidium iodide (PI) assay kit (Sigma, USA). Chondrocytes were incubated with calcein and PI for 20 min in the dark. After rinsing with PBS, the live and dead cells were visualized under a microscope (Olympus BX53, Tokyo, Japan).

Cell counting Kit-8 (CCK-8)

The chondrocytes were seeded in a 96-well plate at a density of 1×10^4 cells per well and cultured for 24 h to allow full adherence. Once confluence was reached, different materials were added to each well for a 24-hour treatment period. Cell viability was then assessed using the CCK-8 assay kit (Beyotime, Shanghai, China), and absorbance at 450 nm was measured using a microplate reader.

Detection of intracellular ROS levels

Chondrocytes were seeded in 24-well plates and incubated overnight. Following 30 min of stimulation with H_2O_2, different materials were added for 24 h of co-culture. DCFH-DA was utilized to detect total ROS, HPF was used to detect ·OH, and DHE was employed to detect O_2^-. Finally, fluorescence microscopy was used to visualize the cells, and various forms of ROS levels were quantified using ImageJ software.

Enzyme-linked immunosorbent assay (ELISA)

The levels of TNF-α and IL-1β in cell supernatant were determined with the ELISA kits (Solarbio) as per the manufacturer's instructions. The absorbance was measured at 450 nm with a microplate reader.

Immunofluorescence staining

Rat chondrocytes were fixed with 4% paraformaldehyde for 15 min, permeabilized with 0.1% Triton X-100 for 5 min, and blocked with 5% bovine serum albumin (BSA) for 1 h. Then, the samples were incubated with the indicated primary antibodies MMP13 (1:200; Affinity; AF5355) overnight at 4 °C. The following day, cells were washed three times with PBS and further visualized under a fluorescence microscope with Alexa 488 secondary antibody at room temperature. DAPI was utilized for nuclear staining.

Western blot

The total protein was extracted from chondrocytes, followed by centrifugation at 12,000 rpm at 4 °C for 10 min, with the protein sample collected from the supernatant. The proteins were then separated via 10% SDS-denaturing polyacrylamide gel electrophoresis (PAGE) and transferred to a PVDF membrane. After washing the membrane with tris-buffered saline (TBS) at room temperature, it was blocked with skimmed milk in TBS for 1 h. The membrane was incubated overnight at 4 °C with primary antibodies: Collagen type II (COL II; 1: 1000; Affinity; AF0135), MMP13 (1: 1000; Affinity; AF5355), IL-1β (1: 1000; Affinity; AF5103), and TNF-α (1: 500; Affinity; AF7014). The following day, the membrane was washed three times with TBS for 10 min each, then incubated for 2 h at room temperature with an HRP-conjugated IgG secondary antibody. After washing with TBS, protein detection was performed using an ECL chemiluminescence detection kit, with GAPDH (1:5000; Affinity; AF7021) as the internal reference. The grey values of the protein bands were quantified through Image J software.

Statistical analysis

The entire dataset was analyzed using SPSS 18.0 and GraphPad Prism 7.0. The experimental results are expressed as the means ± standard deviation (SD). Differences between groups were evaluated using Student's t-test and one-way analysis of variance (ANOVA). A p-value of less than 0.05 was considered statistically significant.

Results

Characterization of Que-Mg NPs and Que-Mg@SA microspheres

Firstly, the synthesis of the Que-Mg complex was evaluated by ultraviolet (UV) and infrared (IR) spectroscopy. Compared to the UV spectrum of Que, the incorporation of Mg^{2+} induced electron transitions, which caused a shift in electron cloud density. Consequently, the absorption peak of Que at 371 nm exhibited a red shift of approximately 60 nm, accompanied by the emergence of a new peak at 430 nm in the Que-Mg spectrum (Fig. S3A), confirming the formation of a complex between Que and Mg. Further verification by IR spectroscopy showed that the C = O stretching vibration of free Que appeared at 1684 cm^{-1}, which shifted to 1636 cm^{-1} in the Que-Mg spectrum, indicating the coordination of the C = O and Mg^{2+}. Moreover, the appearance of an Mg-O stretching vibration peak at 568 cm^{-1} in the Que-Mg spectrum also suggested the formation of the metal complex (Fig. S3B).

These results collectively demonstrate the successful synthesis of Que-Mg NPs.

The structures and morphologies of the synthesized Que-Mg NPs and Que-Mg@SA microspheres were characterized. TEM results indicated that the particle size of Que-Mg NPs was around 30 nm and well dispersed without noticeable aggregation (Fig. 1A). DLS analysis showed the hydrodynamic particle size of Que-Mg NPs was 35.27 ± 2.99 nm, Zeta potential was − (17.65 ± 0.77) mV, and polydispersity index (PDI) was 0.233, displaying a uniform particle size distribution (Fig. 1B-C). Moreover, Que-Mg NPs exhibited almost no fluctuation in their hydrated particle sizes and PDI over a continuous period of seven days, demonstrating their great stability (Fig. 1D). After successfully synthesizing Que-Mg@SA microspheres, the EE% of the microspheres was determined to be (82.71 ± 4.11) %, and the LE% was (10.17 ± 0.51) %. Furthermore, optical microscopy images revealed the morphology of SA (Fig. 1E) and Que-Mg@SA microspheres (Fig. 1F). For particle size comparison,

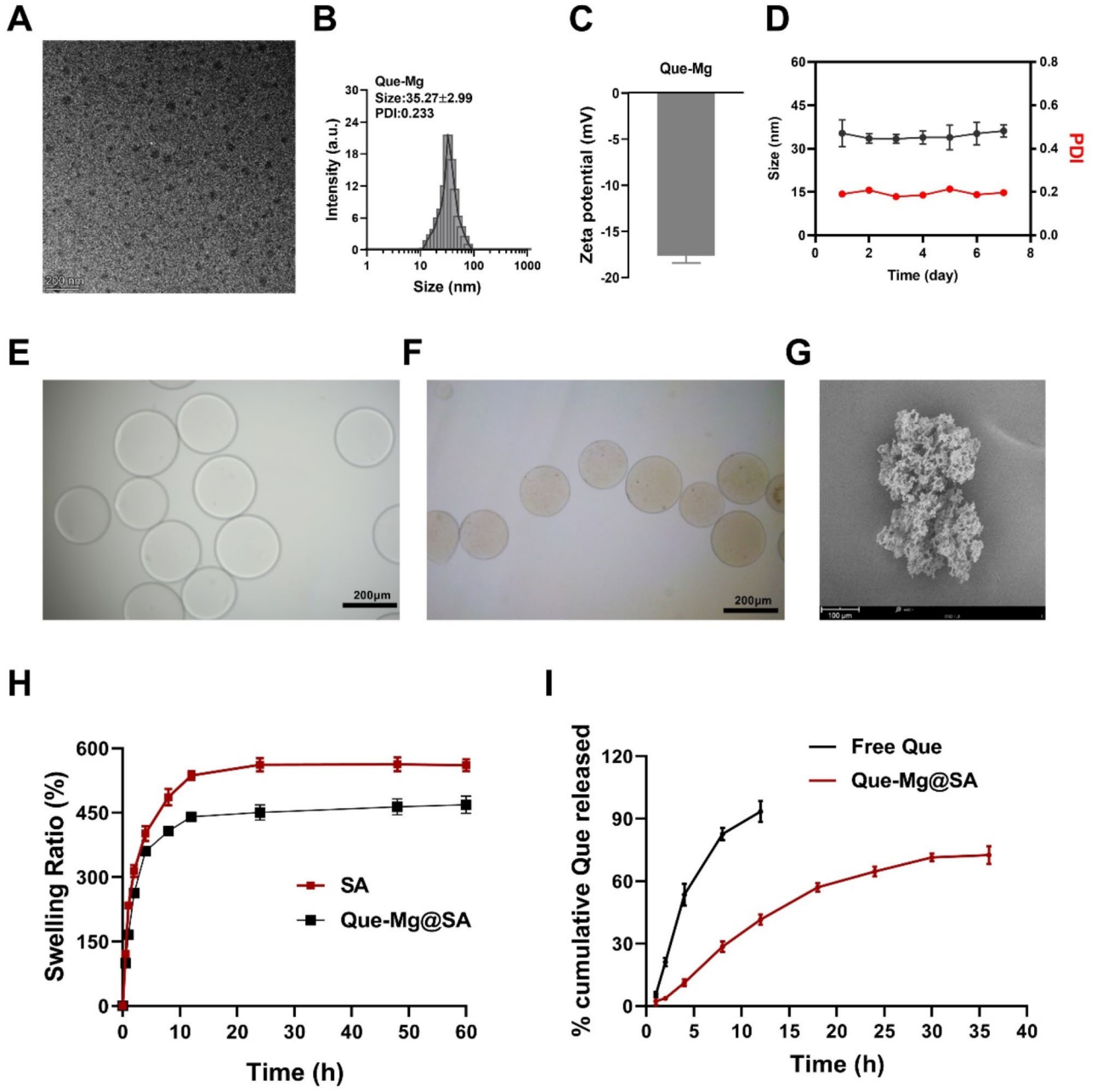

Fig. 1 Characterization of Que-Mg NPs and Que-Mg@SA microspheres. (**A**) TEM image, (**B**) Size distribution, (**C**) zeta potential, and (**D**) Seven-day stability of the Que-Mg NPs; Optical microscope image of (**E**) SA microspheres and (**F**) Que-Mg@SA microspheres; (**G**) SEM image of Que-Mg@SA microspheres; (**H**) The hygroscopicity of SA microspheres and Que-Mg@SA microspheres; (**I**) Release curve of Que

precise statistical analysis using Nano Measure software indicated that the particle sizes of SA and Que-Mg@SA microspheres were approximately 210 nm and 187 nm, respectively, with Que-Mg@SA microspheres exhibiting a significantly smaller diameter than SA microspheres ($p < 0.01$). This size discrepancy is hypothesized to result from the encapsulation process of NPs within the microspheres. When NPs are effectively loaded into the microspheres, they tend to internal voids, leading to a denser overall structure, and this structural compaction is macroscopically reflected as a reduction in microsphere size. Additionally, upon loading Que-Mg nanoparticles, the presence of Que-Mg nanoparticles within the Que-Mg@SA microspheres was distinctly visible, indicating the successful encapsulation of Que-Mg NPs (Fig. 1F). SEM images further demonstrated the porous structure of the synthesized Que-Mg@SA microspheres (Fig. 1G), which not only facilitate drug loading and sustained release but also provide a complex spatial structure and an efficient material exchange system for chondrocytes. Altogether, these aforementioned beneficial characteristics are important for cellular growth and repair at the OA lesion sites.

The water absorbency of microspheres plays a crucial role in lubricating joint surfaces and alleviating inflammatory responses. As shown in Fig. 1H, the swelling ratio results indicate that at 12 h, both the SA microspheres and Que-Mg@SA microspheres exhibited water absorption swelling ratios exceeding 400% in PBS solution, demonstrating that the drug-loaded microspheres still retained strong hygroscopicity capabilities. In addition, the in vitro release results revealed that Que-Mg@SA microspheres exhibited a good sustained release compared to free Que, with the cumulative release of Que reaching (72.58 ± 3.50) % at 36 h (Fig. 1I). The kinetic model fits for the free Que and Que-Mg@SA release profiles were presented in Table S1. This extended residency duration facilitates the maximized therapeutic potential of Que for OA.

Biosafety and cell viability assessment

As depicted in Fig. 2A, the live/dead assay was conducted to assess the biosafety of Que, Que-Mg NPs, SA microspheres, and Que-Mg@SA microspheres on chondrocytes. At one and three days of culture, the density of live cells in the different administration groups continued to increase over time, and there were no dead cells in any group, which was not significantly different compared to the Control group, suggesting that the Que and abovementioned materials possess good biosafety.

In addition, the high concentration of ROS notably promotes chondrocyte apoptosis, cartilage matrix degradation, and the progression of joint inflammation. Among ROS, H_2O_2 is distinguished by its prolonged biological lifespan and its capacity for efficient diffusion both within and between cells [27]. Thus, H_2O_2 was employed in this study to induce inflammation in chondrocytes. To simulate the excessive ROS environment in OA, chondrocytes were exposed to 250 μM H_2O_2 and followed by various treatments, the cell viability of chondrocytes was evaluated using the CCK-8 assay (Fig. 2B) and live/dead assay (Fig. 2C). The results demonstrated that H_2O_2 considerably decreased the cell viability of normal chondrocytes ($p < 0.001$), suggesting that excessive ROS led to chondrocyte apoptosis. Following administration with Que, Que-Mg, or Que-Mg@SA, cell viability improved remarkably compared to the H_2O_2 group ($p < 0.01$, $p < 0.001$). Among all groups, Que-Mg@SA microspheres exhibited the most pronounced improvement in cell viability, substantially restoring the viability of H_2O_2-induced chondrocytes to levels comparable to the Control group (100 ± 8.65%).

ROS scavenging activity of Que-Mg@SA microspheres

The ROS scavenging capacity of Que-Mg@SA microspheres was assessed by measuring the fluorescence intensity of total ROS and common ROS, including ·OH and O_2^-). The results revealed that upon stimulation with 250 μM H_2O_2 markedly elevated ROS production in chondrocytes ($p < 0.001$), as sensitively detected by DCFH-DA, a fluorescent probe for intracellular ROS (Fig. 3A-B). Additionally, the presence of O_2^- and ·OH radicals was identified using DHE and HPF, with the corresponding signals observed in the red and green channels, respectively. By observing the intense and extensive green/red fluorescence signals in the H_2O_2 group, it is clear that a substantial amount of ·OH and O_2^- were generated in most cells upon H_2O_2 stimulation (Fig. 3C-F). Notably, compared to the H_2O_2 group, free Que, Que-Mg, and Que-Mg@SA all weaken the intensity of the increased fluorescence signals induced by H_2O_2, with the Que-Mg@SA group showing the weakest fluorescence.

Anti-inflammatory capacity and regulatory effect on ECM metabolism of Que-Mg@SA microspheres

Studies have reported that when exposed to ROS, chondrocytes trigger an increased production of inflammatory factors, such as TNF-α and IL-1β, resulting in an imbalance in ECM metabolism and a tendency towards ECM degradation [28]. Both ELISA and Western blot analyses revealed remarkably elevated inflammatory levels under H_2O_2 stimulation ($p < 0.001$), as evidenced by the markedly increased IL-1β and TNF-α levels and protein expression. After incubation with Que-Mg@SA, the concentrations of TNF-α and IL-1β in the cell supernatant were restored to levels close to those of normal cells (Fig. 4A-B). Similarly, Western blot analysis confirmed that the expression of IL-1β and TNF-α in chondrocytes

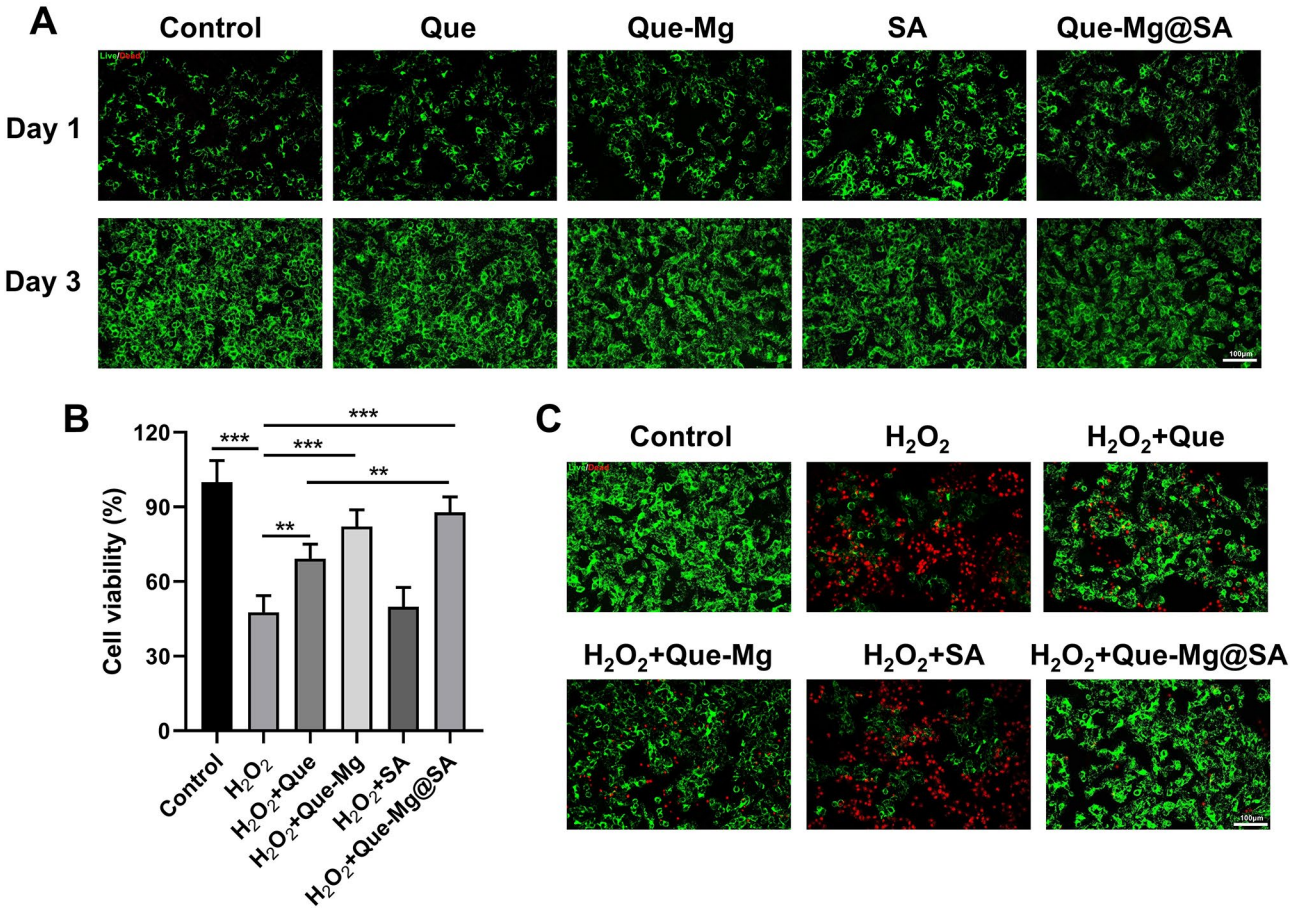

Fig. 2 Que-Mg@SA microspheres possess good biosafety and substantially restore the viability of H_2O_2-induced chondrocytes. (**A**) Live/dead cell staining of Que, Que-Mg NPs, SA microspheres, and Que-Mg@SA microspheres after 1 and 3 days of co-culture with chondrocytes; (**B**) CCK-8 assay and (**C**) live/dead cell staining to evaluate the impact of different administration groups on H_2O_2-induced chondrocyte viability. **, $p < 0.01$; ***, $p < 0.001$

aligned with these findings (Fig. 4C), indicating that Que-Mg@SA could suppress the H_2O_2-induced expression of inflammatory factors.

Moreover, the reduction of inflammatory factors notably promoted ECM synthesis. As shown in Fig. 5A-B, H_2O_2 remarkably upregulated MMP13 expression ($p < 0.001$), whereas incubation with Que-Mg@SA resulted in a substantial decrease in red fluorescence intensity and protein expression ($p < 0.05$), indicating that Que-Mg@SA inhibited MMP13 expression, thereby preventing ECM degradation in chondrocytes. Additionally, under H_2O_2 stimulation, the expression of COL II, a key component of ECM, was considerably reduced ($p < 0.001$). In comparison to the free Que, the intervention with Que-Mg@SA resulted in a more substantial restoration of COL II protein expression to levels comparable to the Control group (Fig. 5B), suggesting that Que-Mg@SA alleviated ECM metabolic imbalance.

Discussion

OA is the most prevalent arthritic disease, with its pathogenesis and progression involving various mechanisms. Aside from joint replacement surgery, OA is generally regarded as incurable [29]. Consequently, there is a pressing need to develop safe and impactful therapeutic strategies to alleviate or halt the progression of OA. Excessive H_2O_2 plays a pivotal role in cellular damage processes, such as chondrocytes, where it inhibits ECM synthesis, induces chondrocyte apoptosis, triggers lipid peroxidation, and promotes the overproduction of inflammatory cytokines, which further contribute to the formation of MMPs [30, 31]. Thus, this study employs H_2O_2-induced OS to establish an OA model, aiming to investigate the therapeutic potential of the synthesized drug delivery system. The results demonstrate that SA microspheres loaded with Que-Mg nanoparticles protect chondrocytes, exhibit anti-inflammatory and antioxidative properties, and notably mitigate ECM metabolic imbalance.

In the present study, we designed and synthesized the Que-Mg@SA microsphere drug delivery system for OA.

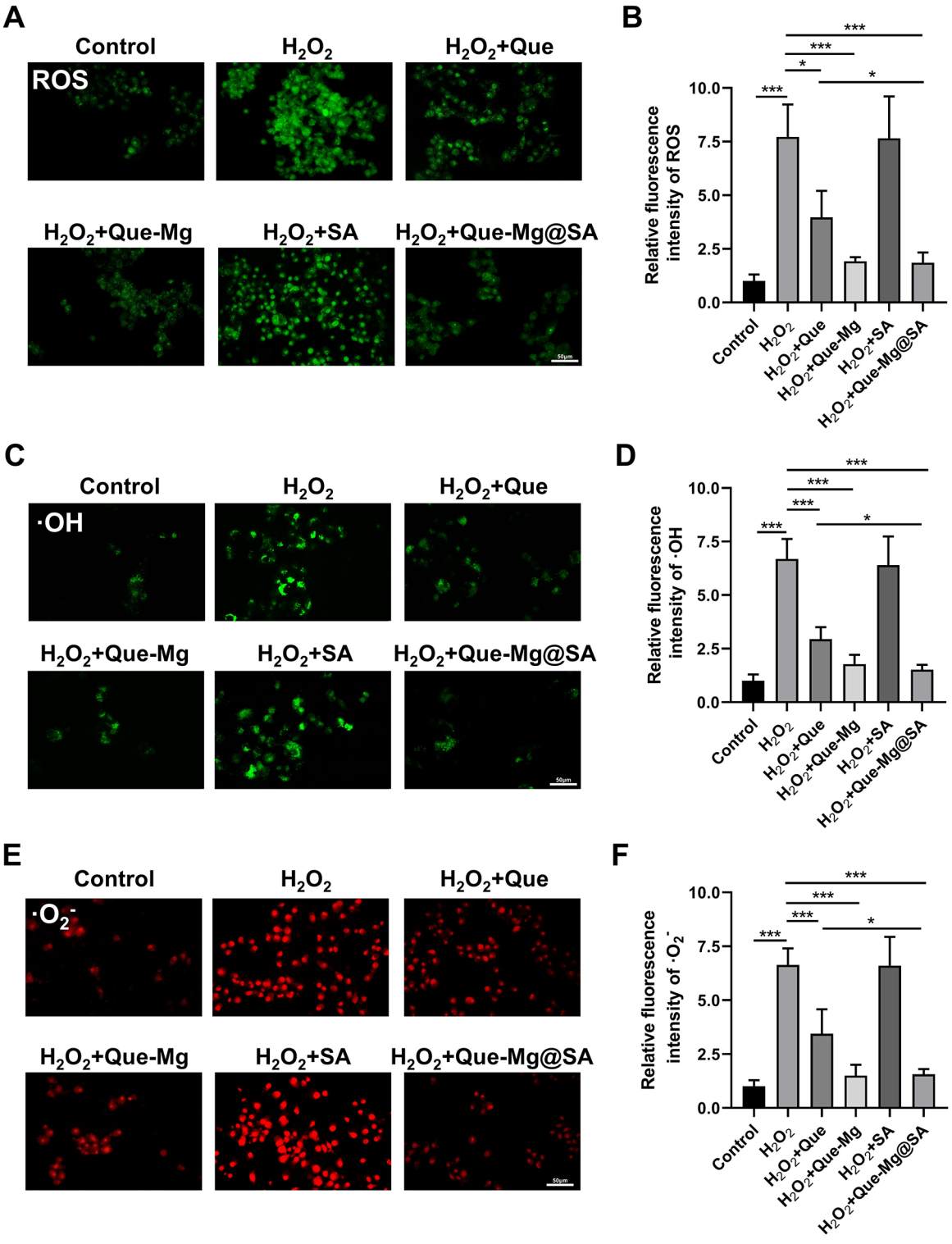

Fig. 3 Que-Mg@SA microspheres effectively attenuate the H_2O_2-induced fluorescence intensity of total ROS and common ROS. Fluorescence micrographs and intensity quantification display the activities of Que-Mg@SA microspheres to scavenge (**A**-**B**) total ROS, (**C**-**D**) ·OH, and (**E**-**F**) $·O_2^-$ in chondrocytes with H_2O_2 treatment. *, $p < 0.05$; ***, $p < 0.001$

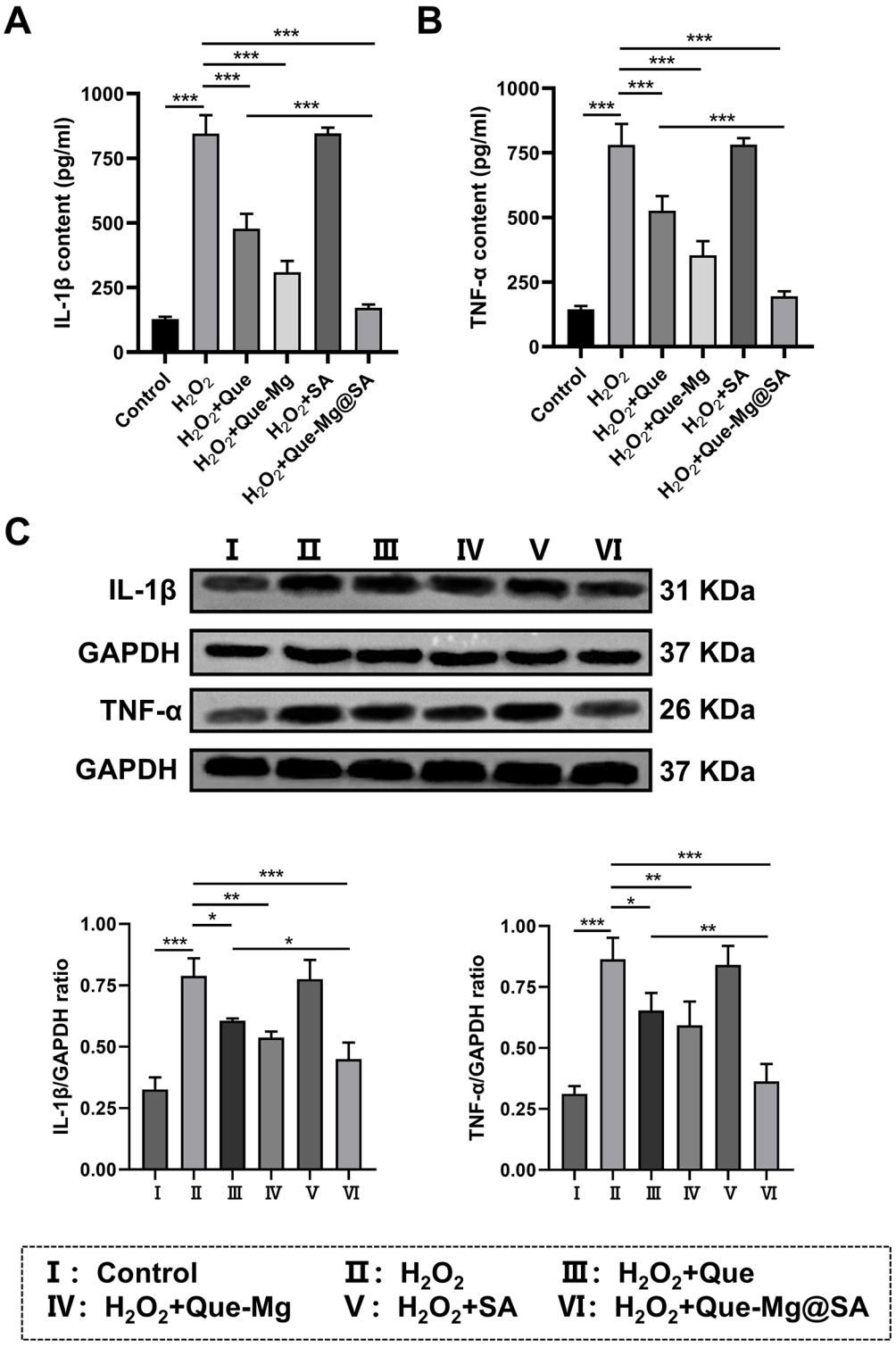

Fig. 4 Que-Mg@SA microspheres suppress the levels and protein expression of IL-1β and TNF-α induced by H_2O_2. ELISA assay detected the levels of (**A**) IL-1β and (**B**) TNF-α; (**C**) Western blot analyzed the protein expression of IL-1β and TNF-α. *, $p < 0.05$; **, $p < 0.01$; ***, $p < 0.001$

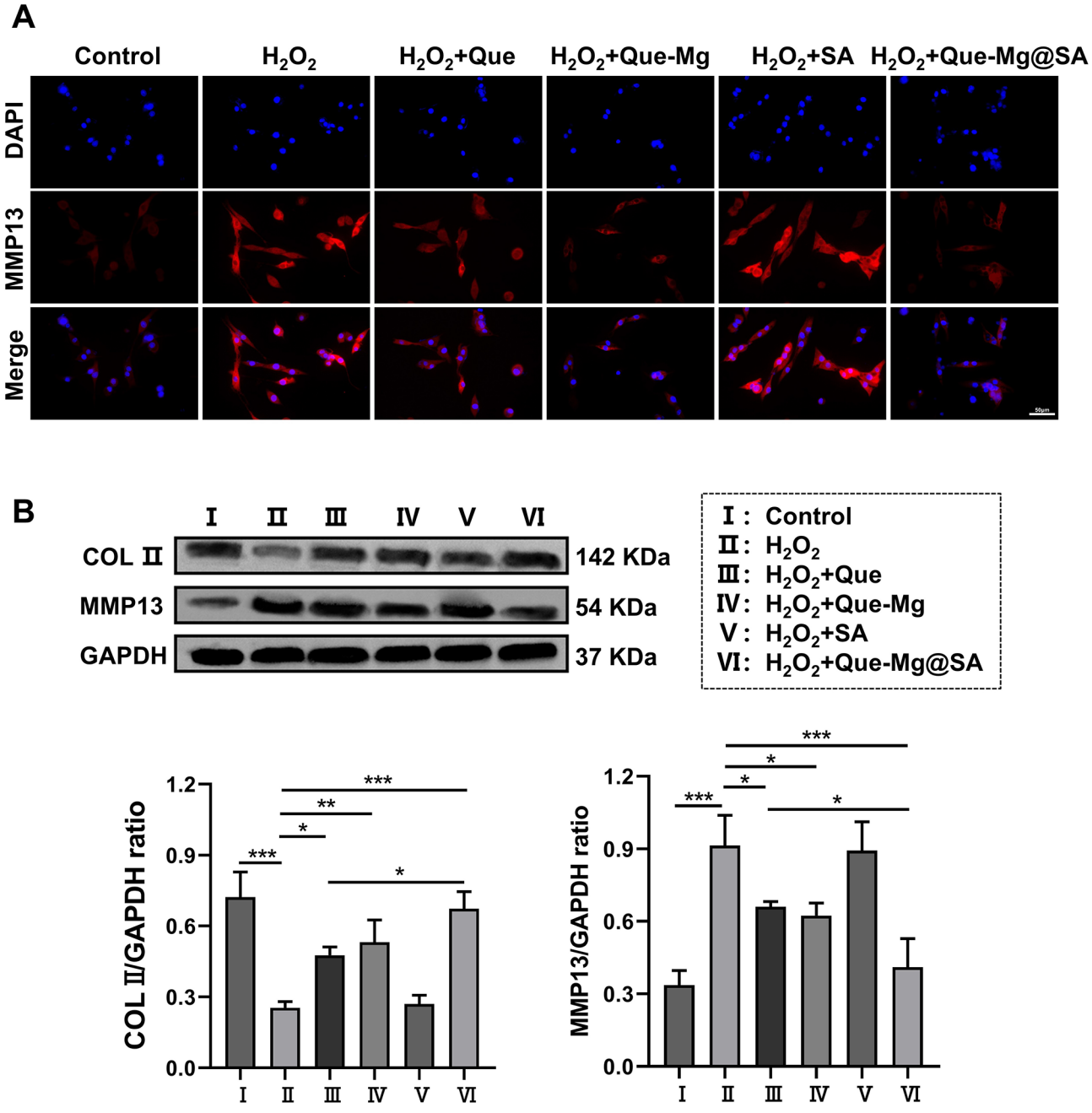

Fig. 5 Que-Mg@SA microspheres alleviate ECM metabolic imbalance. (**A**) Representative immunofluorescence staining images of MMP13; (**B**) Western blot analyzed the protein expression of COL II and MMP13. *, $p < 0.05$; **, $p < 0.01$; ***, $p < 0.001$

Here, characterization results revealed that Que-Mg NPs possess the advantages of nanoscale diameter, exceptional stability, and good dispersibility. What's more, We determined the EE% of Que-Mg@SA to be (82.71 ± 4.11)%, meeting the requirements of the 2020 edition of the Chinese Pharmacopoeia, which stipulates that microsphere EE% must not be less than 80% [32], and the LE% of Que-Mg@SA was (10.17 ± 0.51)%, surpassing the LE% of normal nano-drug formulations (below 10%) [33]. Nano-carriers, possessing suitable size and encapsulation efficiency, can function as micro-environmental modulators, facilitating the targeted and regulated delivery of biomolecules [34]. Furthermore, as an effective carrier, the strong hygroscopic property of SA microspheres is conducive to the reduction of chondrocyte friction and damage on the microsphere surface, thereby promoting chondrocyte repair and proliferation. Additionally, biopolymer carriers are frequently recommended for

controlled and sustained delivery over extended periods [35]. As anticipated, the drug release profiles of free Que and Que-Mg@SA demonstrate that the utilization of the SA microsphere prevents rapid drug depletion and facilitates sustained, efficient release at the osteoarticular site. This controlled, extended drug delivery within the joint eliminates the requirement for frequent injections while ensuring consistent therapeutic efficacy.

Biological safety is an essential prerequisite for the clinical use of nanomaterials. Live/dead cell staining results proved that Que, Que-Mg NPs, SA microspheres, and Que-Mg@SA microspheres exhibit good biocompatibility and an absence of cytotoxicity on chondrocytes, which is a prerequisite for in vivo experiments and applications in clinical practice [36]. Prior studies have identified OS-induced chondrocyte apoptosis as a key factor in the progression of OA [37]. Thus, cell viabilities under various treatment conditions were evaluated through CCK-8 and AM/PI analyses. The results confirmed that Que-Mg@SA microspheres inhibited chondrocyte apoptosis, offering superior protection against the harmful influence of H_2O_2 compared to free Que. Moreover, the imbalance between ROS production and the protective antioxidant mechanisms in chondrocytes is a critical factor in the progression of OA [38]. The outcomes of our study revealed that H_2O_2-induced OS notably elevated ROS levels in chondrocytes, a process suppressed by Que-Mg@SA, illustrating that SA microspheres loaded with Que-Mg NPs exhibited substantial efficacy in scavenging various forms of ROS. Mg^{2+} can promote the synthesis of cartilage matrix, yet OS exacerbates inflammation, thereby compromising the therapeutic effect of Mg^{2+} in OA [39]. Que is a potent free radical scavenger with significant antioxidant properties, that can neutralize ROS and alleviate oxidative damage to chondrocytes, thereby protecting their structure and function [40]. By combining Que with Mg^{2+} to form Que-Mg@SA, the synergistic benefits of both are fully realized. On one hand, Que scavenges ROS, mitigating OS-induced damage to chondrocytes, and enhancing the role of Mg^{2+} in cartilage matrix synthesis and repair. On the other hand, the addition of Mg^{2+} further stimulates chondrocyte metabolism and repair, boosting Que's antioxidant effects. Therefore, Que-Mg@SA microspheres hold considerable potential in improving OA by increasing chondrocyte viability and mitigating OS in chondrocytes.

ROS in deteriorating joints disrupts cellular processes and activates pro-inflammatory factors [41], with IL-1β and TNF-α being the most prominent contributors. Our in vitro experimental results revealed that H_2O_2 exposure substantially upregulated the levels of TNF-α and IL-1β, whereas Que-Mg@SA considerably mitigated this inflammatory response. In addition, these pro-inflammatory cytokines are key drivers of ECM degradation, a hallmark of OA [42], with MMPs serving as the primary enzymes responsible for the degradation of ECM in OA chondrocytes [43]. Among the MMP family, MMP-13 exhibits the highest potency in degrading the chondrogenic gene COL II [44]. In our research, H_2O_2 significantly upregulated MMP-13 gene expression in chondrocytes, while simultaneously suppressing the expression of COL II. This imbalance between MMP13 and COL II contributes to ECM degradation and accelerates cartilage deterioration [45]. However, the Que-Mg@SA intervention reversed these trends, indicating that the damaged chondrocytes were protected against OS.

Conclusions

In the present study, we introduce an innovative therapeutic strategy by synthesizing Que-Mg NPs integrated with SA microspheres for treating an OA cell model. The Que-Mg@SA microspheres demonstrated an exceptional water absorption capacity and sustained drug release properties. Additionally, in vitro cellular assays revealed that the biocompatible Que-Mg@SA microspheres markedly restored chondrocyte viability, scavenged H_2O_2-induced excessive ROS, reduced the levels of inflammatory cytokines, upregulated cartilage anabolic gene expression, downregulated cartilage catabolic protease gene expression, and maintained the metabolic balance of cartilage tissue. Overall, the functionalized microspheres developed herein hold great promise as a drug delivery system for OA treatment and potentially other biomedical applications, yet further investigation through in vivo studies, followed by clinical trials, is essential before the microspheres are authentically used in the clinical management of OA.

Supplementary Information

The online version contains supplementary material available at https://doi.org/10.1186/s13018-025-05698-z.

Supplementary Material 1: The standard calibration curve of drug release studies.

Supplementary Material 2: The concentration of Que was screened from the preliminary experiment using the CCK-8 assay.

Supplementary Material 3: The successful synthesis of Que-Mg NPs was confirmed by the (A) ultraviolet (UV) and (B) infrared (IR) spectrums.

Supplementary Material 4: Table S1. The kinetic model fits the free Que and Que-Mg@SA release profiles

Acknowledgements
Not applicable.

Author contributions
Conceptualization ideas, JC and GW; validation verification, JW; formal analysis, JC and GW; data curation, JC and GW, and JW; writing - original draft preparation, JC and GW; writing - review & editing, ZJ; visualization preparation, ZJ; funding acquisition, JW. All authors have read and agreed to the published version of the manuscript.

Funding
This work was supported by Natural Science Foundation of Hubei Province (grant number 2022CFB551) and Key Scientific Research Project of Xianning Central Hospital (grant number 2023XYA001).

Data availability
No datasets were generated or analysed during the current study.

Declarations

Ethics approval and consent to participate
Not applicable.

Consent for publication
Not applicable.

Competing interests
The authors declare no competing interests.

Author details
[1]Department of Orthopedics, Xianning Central Hospital, The First Affiliated Hospital of Hubei University of Science and Technology, NO. 228 Jingui Road, Xian'an District, Xianning, Hubei 437100, China

Received: 13 December 2024 / Accepted: 9 March 2025
Published online: 20 March 2025

References

1. Hootman JM, Helmick CG, Barbour KE, Theis KA, Boring MA. Updated projected prevalence of self-reported doctor-diagnosed arthritis and arthritis-attributable activity limitation among US adults, 2015–2040. Arthritis Rheumatol. 2016;68:1582–7.
2. Kolasinski SL, Neogi T, Hochberg MC, Oatis C, Guyatt G, Block J, et al. 2019 American college of rheumatology/arthritis foundation guideline for the management of osteoarthritis of the hand, hip, and knee. Arthritis Rheumatol. 2020;72:220–33.
3. Li G, Liu S, Chen Y, Zhao J, Xu H, Weng J, et al. An injectable liposome-anchored teriparatide incorporated Gallic acid-grafted gelatin hydrogel for osteoarthritis treatment. Nat Commun. 2023;14:3159.
4. Yu H, Gao R, Liu Y, Fu L, Zhou J, Li L. Stimulus-Responsive hydrogels as drug delivery systems for inflammation targeted therapy. Adv Sci. 2024;11:2306152.
5. Zhang H, Huang J, Alahdal M. Exosomes loaded with chondrogenic stimuli agents combined with 3D Bioprinting hydrogel in the treatment of osteoarthritis and cartilage degeneration. Biomed Pharmacother. 2023;168:115715.
6. Katz JN, Arant KR, Loeser RF. Diagnosis and treatment of hip and knee osteoarthritis: a review. JAMA. 2021;325:568–78.
7. Zhu R, Wang Y, Ouyang Z, Hao W, Zhou F, Lin Y, et al. Targeting regulated chondrocyte death in osteoarthritis therapy. Biochem Pharmacol. 2023;215:115707.
8. Chen B, Wang L, Xie D, Wang Y. Exploration and breakthrough in the mode of chondrocyte death-A potential new mechanism for osteoarthritis. Biomed Pharmacother. 2024;170:115990.
9. Mai J, Xiao J, Ma Y, Gong D, Li J. Arctiin alleviates the progression of osteoarthritis by regulating the cholesterol metabolic pathway. Sci Rep. 2025;15:263.
10. Beekhuizen M, Bastiaansen-Jenniskens YM, Koevoet W, Saris DB, Dhert WJ, Creemers LB, et al. Osteoarthritic synovial tissue Inhibition of proteoglycan production in human Osteoarthritic knee cartilage: establishment and characterization of a long-term cartilage–synovium coculture. Arthr Rhuem. 2011;63:1918–27.
11. Khan AK, Kousar S, Tungmunnithum D, Hano C, Abbasi BH, Anjum S. Nano-elicitation as an effective and emerging strategy for in vitro production of industrially important flavonoids. Appl Sci. 2021;11:1694.
12. Maleki SJ, Crespo JF, Cabanillas B. Anti-inflammatory effects of flavonoids. Food Chem. 2019;299:125124.
13. Li W, Wang Y, Tang Y, Lu H, Qi Y, Li G, et al. Quercetin alleviates osteoarthritis progression in rats by suppressing inflammation and apoptosis via Inhibition of IRAK1/NLRP3 signaling. J Inflamm Res. 2021;14:3393–403.
14. Goyal A, Agrawal N. Quercetin: a potential candidate for the treatment of arthritis. Curr Mol Med. 2022;22:325–35.
15. Wei B, Zhang Y, Tang L, Ji Y, Yan C, Zhang X. Protective effects of Quercetin against inflammation and oxidative stress in a rabbit model of knee osteoarthritis. Drug Dev Res. 2019;80:360–7.
16. Maudens P, Jordan O, Allémann E. Recent advances in intra-articular drug delivery systems for osteoarthritis therapy. Drug Discovery Today. 2018;23:1761–75.
17. Li Y, Zhao S, Li S, Ge Y, Wang R, Zheng L, et al. Surface engineering of biodegradable magnesium alloys for enhanced orthopedic implants. Small. 2019;15:1904486.
18. Bai R, Miao MZ, Li H, Wang Y, Hou R, He K, et al. Increased Wnt/β-catenin signaling contributes to autophagy Inhibition resulting from a dietary magnesium deficiency in injury-induced osteoarthritis. Arthritis Res Therapy. 2022;24:165.
19. Sánchez AHM, Omidi M, Wurlitzer M, Fuh MM, Feyerabend F, Schlüter H, et al. Proteome analysis of human mesenchymal stem cells undergoing chondrogenesis when exposed to the products of various magnesium-based materials degradation. Bioactive Mater. 2019;4:168–88.
20. Chen K, Xie X, Tang H, Sun H, Qin L, Zheng Y, et al. In vitro and in vivo degradation behavior of Mg–2Sr–Ca and Mg–2Sr–Zn alloys. Bioactive Mater. 2020;5:275–85.
21. Yao H, Xu J, Zheng N, Wang J, Mok S, Lee Y, et al. Intra-articular injection of magnesium chloride attenuates osteoarthritis progression in rats. Osteoarthr Cartil. 2019;27:1811–21.
22. Singh H, Knapik DM, Polce EM, Eikani CK, Bjornstad AH, Gursoy S, et al. Relative efficacy of intra-articular injections in the treatment of knee osteoarthritis: a systematic review and network meta-analysis. Am J Sports Med. 2022;50:3140–8.
23. Dhamecha D, Movsas R, Sano U, Menon JU. Applications of alginate microspheres in therapeutics delivery and cell culture: past, present and future. Int J Pharm. 2019;569:118627.
24. Karpov AA, Anikin NA, Mihailova AM, Smirnov SS, Vaulina DD, Shilenko LA, et al. Model of chronic thromboembolic pulmonary hypertension in rats caused by repeated intravenous administration of partially biodegradable sodium alginate microspheres. Int J Mol Sci. 2021;22:1149.
25. Zhou Y, Yang F, Zhou H, Lv S. Alginate/Carboxymethyl Chitosan Core-Shell microspheres coloaded with doxorubicin/docetaxel reverse chemotherapy resistance in anaplastic thyroid carcinoma. Thyroid. 2024;34:856–70.
26. Yan Y, Lu A, Dou Y, Zhang Z, Wang XY, Zhai L, et al. Nanomedicines reprogram synovial macrophages by scavenging nitric oxide and Silencing CA9 in progressive osteoarthritis. Adv Sci (Weinh). 2023;10:e2207490.
27. Behera SS, Pramanik K, Nayak MK. Recent advancement in the treatment of cardiovascular diseases: conventional therapy to nanotechnology. Curr Pharm Des. 2015;21:4479–97.
28. Chen Q, Jin Y, Chen T, Zhou H, Wang X, Wu O, et al. Injectable nanocomposite hydrogels with enhanced lubrication and antioxidant properties for the treatment of osteoarthritis. Mater Today Bio. 2024;25:100993.
29. Hawker G, Lohmander L. What an earlier recognition of osteoarthritis can do for OA prevention. Osteoarthr Cartil. 2021;29:1632–4.
30. Guo D, Yu M, Guo H, Zeng M, Shao Y, Deng W, et al. Panax Notoginseng saponins inhibits oxidative stress- induced human nucleus pulposus cell apoptosis and delays disc degeneration in vivo and in vitro. J Ethnopharmacol. 2024;319:117166.
31. Gao G, Ding H, Zhuang C, Fan W. Effects of hesperidin on H_2O_2-Treated chondrocytes and cartilage in a rat osteoarthritis model. Med Sci Monit. 2018;24:9177–86.
32. The China Pharmacopeial Convention. Pharmacopoeia of the People's Republic of China 2020. China Medical Science; 2020.
33. Xu Z, Lin H, Dai J, Wen X, Yu X, Xu C, et al. Protein-nanoparticle co-assembly supraparticles for drug delivery: ultrahigh drug loading and colloidal stability, and instant and complete lysosomal drug release. Int J Pharm. 2024;658:124231.
34. Palazzo I, Lamparelli EP, Ciardulli MC, Scala P, Reverchon E, Forsyth N, et al. Supercritical emulsion extraction fabricated PLA/PLGA micro/nano carriers for growth factor delivery: release profiles and cytotoxicity. Int J Pharm. 2021;592:120108.
35. Ciaglia E, Montella F, Trucillo P, Ciardulli MC, Di Pietro P, Amodio G, et al. A bioavailability study on microbeads and nanoliposomes fabricated by dense carbon dioxide technologies using human-primary monocytes and flow cytometry assay. Int J Pharm. 2019;570:118686.

36. Han Y, Yang J, Zhao W, Wang H, Sun Y, Chen Y, et al. Biomimetic injectable hydrogel microspheres with enhanced lubrication and controllable drug release for the treatment of osteoarthritis. Bioact Mater. 2021;6:3596–607.
37. Pan Y, Chen D, Lu Q, Liu L, Li X, Li Z. Baicalin prevents the apoptosis of endplate chondrocytes by inhibiting the oxidative stress induced by H2O2. Mol Med Rep. 2017;16:2985–91.
38. Ansari MY, Ahmad N, Haqqi TM. Oxidative stress and inflammation in osteoarthritis pathogenesis: role of polyphenols. Biomed Pharmacother. 2020;129:110452.
39. Yao H, Xu J, Wang J, Zhang Y, Zheng N, Yue J, et al. Combination of magnesium ions and vitamin C alleviates synovitis and osteophyte formation in osteoarthritis of mice. Bioact Mater. 2021;6:1341–52.
40. Liu M, Gao M, Shi X, Yin Y, Liu H, Xie R, et al. Quercetin attenuates SiO(2)-induced ZBP-1-mediated PANoptosis in mouse neuronal cells via the ROS/TLR4/NF-kappab pathway. J Environ Manage. 2024;370:122948.
41. Forrester SJ, Kikuchi DS, Hernandes MS, Xu Q, Griendling KK. Reactive oxygen species in metabolic and inflammatory signaling. Circul Res. 2018;122:877–902.
42. Kang L-J, Yoon J, Rho JG, Han HS, Lee S, Oh YS, et al. Self-assembled hyaluronic acid nanoparticles for osteoarthritis treatment. Biomaterials. 2021;275:120967.
43. Li H, Wang D, Yuan Y, Min J. New insights on the MMP-13 regulatory network in the pathogenesis of early osteoarthritis. Arthritis Res Therapy. 2017;19:248.
44. Perotto JH, Camejo FA, Doetzer AD, Almeida LE, Azevedo M, Olandoski M, et al. Expression of MMP-13 in human temporomandibular joint disc derangement and osteoarthritis. Cranio®. 2018;36:161–6.
45. Hu Q, Ecker M. Overview of MMP-13 as a promising target for the treatment of osteoarthritis. Int J Mol Sci. 2021;22:1742.

Publisher's note